

Production of magnetic energy by macroscopic turbulence in GRB afterglows

Lorenzo Sironi
Jeremy Goodman

Princeton University Observatory, Princeton, NJ 08544

jeremy@astro.princeton.edu

ABSTRACT

Afterglows of gamma-ray bursts are believed to require magnetic fields much stronger than that of the compressed pre-shock medium. As an alternative to microscopic plasma instabilities, we propose amplification of the field by macroscopic turbulence excited by the interaction of the shock with a clumpy pre-shock medium, for example a stellar wind. Using a recently developed formalism for localized perturbations to an ultra-relativistic shock, we derive constraints on the lengthscale, amplitude, and volume filling factor of density clumps required to produce a given magnetic energy fraction within the expansion time of the shock, assuming that the energy in the field achieves equipartition with the turbulence. Stronger and smaller-scale inhomogeneities are required for larger shock Lorentz factors. Hence it is likely that the magnetic energy fraction evolves as the shock slows. This could be detected by monitoring the synchrotron cooling frequency if the radial density profile ahead of the shock, smoothed over clumps, is known.

1. Introduction

Since their discovery, gamma-ray burst afterglows have been attributed to synchrotron radiation from the forward shock wave (Meszaros & Rees 1997), although it has been recently argued (Uhm & Beloborodov 2007; Genet et al. 2007) that observations might support a model in which the forward shock is invisible and the afterglow is emitted by a long-lived reverse shock in the burst ejecta. Assuming anyway a forward-shock origin for the afterglow emission, it is difficult to account for the magnetic energy density behind the forward shock by simple compression of the pre-shock field. Interstellar magnetic energy densities are typically comparable to thermal pressures and are therefore a fraction $\epsilon_{B,0} \equiv \rho_{\text{mag},0}/\rho_0 = 10^{-9} - 10^{-7}$ of the total internal energy density when rest mass is included. It is possible that the pre-shock medium is the stellar wind of the burst progenitor; while the magnetic energy fraction in winds is less well known, it is unlikely to be much larger than this. Simply compressing the medium would produce approximately the same ratio ρ_{mag}/ρ behind the shock. Instead, phenomenological models of afterglow light curves typically require $\epsilon_B = 10^{-3} - 10^{-1}$ (Panaitescu & Kumar 2002; Yost et al. 2003; Panaitescu 2005). It follows that the magnetic energy per baryon must be increased by $\sim 10^4 - 10^8$.

In fact, gamma-ray burst (hereafter GRB) afterglows present the most compelling case among astrophysical collisionless shocks for prompt creation of magnetic energy. The synchrotron emission from supernova remnants is generally consistent with compression of the interstellar field, although some modest additional amplification may be required in particular cases (Völk et al. 2005). We focus here on GRB afterglows rather than GRB internal shocks, which also emit by some combination of synchrotron and synchrotron self-Compton, because it may be that the burst ejecta are magnetically dominated (Coburn & Boggs 2003; Zhang et al. 2003), and so the internal shock emission is driven by the progenitor magnetic field.

The leading hypothesis for field amplification in GRB afterglows is the relativistic Weibel instability, which extracts free energy from the anisotropy of the particles’ velocity distribution function, producing filamentary currents aligned with the shock normal; these currents are responsible for the creation of transverse magnetic fields (Medvedev & Loeb 1999). This process is able to violate MHD flux-freezing because it occurs on a microscopic scale—the relativistic electron or ion skin depth—where the inertia of individual charged particles is significant. While the Weibel instability provides a plausible mechanism to isotropize the particle velocities, it is unclear whether the small-scale fields that it produces can survive mutual annihilation long enough to explain the observed synchrotron afterglow emission. Several groups (Silva et al. 2003; Frederiksen et al. 2004; Spitkovsky 2005) have attempted to simulate the long-term nonlinear outcome of the instability, but a consensus on this question has not been achieved yet (Waxman 2006, and references therein). One might have thought that if this instability were the source of post-shock fields, then ϵ_B should have a universal value for highly relativistic, highly collisionless shocks. Yet, while ϵ_B is modeled by a constant for individual GRB afterglows, it seems to vary from one afterglow to another (Panaitescu & Kumar 2002; Yost et al. 2003; Panaitescu 2005).

In this paper, we explore a traditional magnetohydrodynamic explanation for magnetic field growth: turbulence. It is well known in non-relativistic fluid dynamics that oblique shocks produce or alter the vorticity of a fluid (Ishizuka et al. 1964). In this paper we will show that the same is true for an ultra-relativistic shock passing over density inhomogeneities in the pre-shock circumburst medium. The formalism described in a previous paper (Goodman & MacFadyen 2007) has let us define the vorticity created in an ultra-relativistic fluid in which the energy-momentum tensor can be approximated by that of an ideal fluid with pressure equal to one third of the proper energy density ($P = \rho/3$). In the same work, we have introduced a remarkably simple but accurate general approximation for the local modulation of the shock Lorentz factor (Γ) by pre-shock density inhomogeneities; within this approximation, it is not necessary to follow the details of the flow far downstream in order to predict the evolution of the shock, provided that $\Gamma \gg 1$, that the pre-shock pressure is negligible and that the post-shock pressure satisfies $P = \rho/3$. This approximation, which is modeled on non-relativistic results described by Whitham (1974), reproduces exactly the self-similar evolution of Γ for a shock advancing into a cold pre-shock medium with a power-law density profile in planar, cylindrical, or spherical symmetry (Sari 2006). More importantly for the present purpose, it allows us to estimate the post-shock vorticity resulting from a prescribed pre-

shock density that varies along as well as perpendicular to the shock normal. Given the vorticity, we divide the post-shock velocities, which are marginally non-relativistic in the average post-shock rest frame, into vortical and non-vortical parts. We presume that the energy density in vortical motions is a measure of the magnetic energy density that will eventually result after the eddies wind up the field to the point where its backreaction on the turbulence becomes important. These methods are described in §II.

In §III, we briefly review the present state of knowledge concerning the density inhomogeneities that may exist ahead of the shock. Both the amplitude and the lengthscale of the inhomogeneities are important. The former controls the amount of vortical energy—and then of magnetic energy—that is produced, while the latter determines the eddy-turnover time of the turbulence, which—when multiplied by the number of eddy rotations necessary to amplify the field up to the observed ϵ_B —must be less than the shock deceleration time, so that the field can be significantly amplified before adiabatic expansion reduces the particle energies available to be radiated. The uncertainties are large because one doesn’t know whether the pre-shock medium is more like a stellar wind or like some component of the Galactic interstellar medium, and because the lengthscales of interest are too small ($\lesssim 10^{14}$ cm) to be directly resolved even in the interstellar medium. Inhomogeneities on somewhat larger scales have been invoked to explain undulations in afterglow light curves (Wang & Loeb 2000; Lazzati et al. 2002; Schaefer et al. 2003; Nakar et al. 2003).

In §IV, we use the formalism of §II to characterize the density contrasts and lengthscales that pre-shock clumps should have in order to amplify the magnetic field up to the observed value, in the light of the circumburst picture outlined in §III. We find that, for smaller shock Lorentz factors, the constraints on clump sizes and overdensities become less stringent; as a consequence, the magnetic energy fraction produced by pre-shock clumps *via* macroscopic turbulence is expected to evolve as the shock slows down. In §V, we comment on the plausibility of our proposed mechanism to explain the magnetic field amplification in GRB afterglows and we discuss how the results obtained in §IV could be tested by inferring the time dependence of ϵ_B from the time evolution of the observed synchrotron cooling frequency as the shock ages.

2. Geometrical Shock Dynamics

The evolution of a shock advancing into an inhomogeneous medium depends, in principle, upon the details of the downstream flow behind the shock and of the “piston” that drives it. Geometrical Shock Dynamics (hereafter GSD) is an approximation for this evolution in which only the conditions at the shock appear explicitly. Originally formulated by Whitham (1974) for non-relativistic fluids, GSD has been extended by Goodman & MacFadyen (2007, hereafter Paper I) to strong ($\Gamma \gg 1$) ultra-relativistic shocks advancing into an ideal fluid whose pressure is negligible ahead of the shock, but one third of its proper energy density behind the shock ($P = \rho/3$).

The fundamental approximation of GSD is to evaluate the forward-going Riemann character-

istics in the post-shock flow as if that flow were (i) isentropic and (ii) homogeneous far downstream with properties determined by the mean shock speed and the mean pre-shock density. Actually, pre-shock density inhomogeneities lead to post-shock entropy variations, so assumption (i) is wrong in principle, but it turns out to be a useful fiction. In this respect, an ultra-relativistic flow has the advantage that since pressure depends only on energy density and not on any other thermodynamic variable (such as the proper number density of baryons, N), the actual entropy is irrelevant to the Riemann characteristics, which therefore enjoy exact Riemann invariants. So assumption (i) is well justified except insofar as it may be compromised by secondary shocks created by the inhomogeneities themselves behind the main shock. Assumption (ii) is reasonable when pre-shock density inhomogeneities are small in lengthscale, so that they may be expected to average out far downstream.

With assumption (i), the Riemann invariant on the forward characteristics has the same value just behind the shock as it does far downstream, and therefore, with assumption (ii), the same value that it would have in the mean flow. Together with the jump conditions across the shock, this provides a relation between the local Lorentz factor of the shock, Γ , and the proper pre-shock energy density $\rho_0 \approx mN_0c^2$, in which N_0 is the proper number density of nucleons ahead of the shock and m is the rest mass per nucleon. In the essentially one-dimensional case that ρ_0 varies along the shock normal but not perpendicular to it, the ultra-relativistic GSD relation for the response of the shock Lorentz factor Γ to localized and transitory variations in the pre-shock density ρ_0 becomes (Paper I)

$$\Gamma = \bar{\Gamma} \left(\frac{\rho_0}{\bar{\rho}_0} \right)^{-\lambda} \quad \text{where } \lambda \equiv \sqrt{3} - \frac{3}{2} \approx 0.232 \quad (1)$$

and the corresponding change in the post-shock pressure is

$$P = \bar{P} \left(\frac{\rho_0}{\bar{\rho}_0} \right)^{1-2\lambda} \approx \bar{P} \left(\frac{\rho_0}{\bar{\rho}_0} \right)^{0.536}, \quad (2)$$

where the overbars indicate mean values. As in non-relativistic GSD, these relations can be extended to multidimensional flows in which ρ_0 varies laterally as well as longitudinally (with respect to the shock normal), causing convergence or divergence of the shock normals. Relations (1) and (2) are then modified by factors involving the ratio of the local shock area to its mean value (Paper I). It is shown, however, that these corrections are of higher order in Γ^{-1} unless the density contrasts are $\sim O(\Gamma)$. For the conditions contemplated in this paper, eqs. (1) and (2) will be adequate even in two or three dimensions.

As in the original non-relativistic theory, rigorous error estimates for ultra-relativistic GSD are difficult. Informally, the following conditions are probably necessary for the approximation to be useful. First, the pre-shock medium should be cold, meaning that pre-shock pressure satisfies $P_0 \ll \rho_0$ and that internal velocities are $\ll c$; this is very likely true of the external forward shocks of GRBs. Second, the lengthscales of the pre-shock inhomogeneities should be small compared to the shock radius, so that the shock responds to local perturbations before conditions far downstream have time to react. Third, since Γ^{-1} is used as a small parameter, the pre-shock density fluctuations

should not be so large as to cause the shock to become sub-relativistic, *i.e.* one requires $\rho_0/\bar{\rho}_0 \ll \bar{\Gamma}^{1/\lambda}$. Finally, transitions in density should not be so abrupt as to cause strong reverse shocks, which would alter the forward shock dynamics. Paper I describes tests of ultra-relativistic GSD by comparison with exact self-similar solutions (some of which it reproduces exactly) and with numerical simulations. The latter indicate, for example, that eqs. (1) and (2) are in error by only a few percent for a $\bar{\Gamma} = 10^2$ shock encountering overdensities as large as $\rho_0/\bar{\rho}_0 \lesssim 30$.

2.1. Relativistic vorticity

This subsection is independent of GSD. We review the meaning of enthalpy current and vorticity in ideal relativistic fluids, especially those with the ultra-relativistic equation of state $P = \rho/3$.

When the shock passes over a local density excess—considered, for simplicity, in isolation from other inhomogeneities—the resulting post-shock velocities are of two kinds. First, since the shocked clump is overpressured compared to its post-shock surroundings [eq. (2)], it will expand and drive an outgoing pressure wave. If the density contrast of the clump is small, then the wave is essentially a linear disturbance from the start and travels at the sound speed, $c/\sqrt{3}$, in the rest frame of the mean post-shock flow; waves launched by large overdensities will be somewhat faster and may steepen into secondary shocks, but whatever its strength, the pressure wave rapidly departs its source. Overlapping pressure waves launched by many distant clumps may contribute significant local velocity perturbations, but, because of their oscillatory nature, intuition suggests that these velocities will not secularly amplify the magnetic field (except insofar as secondary shocks may contribute to vorticity—see §IV). It would be interesting to test this expectation in numerical simulations.

Unless the density excess is constant along the shock front, the post-shock velocity field will also contain a vortical component, whose strength is estimated below for an initially spherical overdensity with a gaussian radial profile. As shown in Paper I, the equation of state $P = \rho/3$ allows some freedom in how one defines relativistic vorticity, but to be useful in constraining the evolution of the flow, the vorticity should be associated with a conservation law such as Kelvin’s Circulation Theorem,

$$\frac{d}{dt} \oint_C H_\mu dx^\mu = 0, \quad (3)$$

where C is a closed contour comoving with the fluid four-velocity U^μ , and $H^\mu = hU^\mu$ for an appropriate thermodynamic function h (see below). Equation (3) is equivalent to

$$\frac{\partial \boldsymbol{\omega}}{\partial t} - \boldsymbol{\nabla} \times (\mathbf{v} \times \boldsymbol{\omega}) = 0, \quad \boldsymbol{\omega} \equiv c \boldsymbol{\nabla} \times \mathbf{H}, \quad (4)$$

where $v^i \equiv cU^i/U^0$ is the three-velocity of the fluid, and \mathbf{H} is the spatial part of H^μ . Although formally identical to the non-relativistic vorticity equation and written with three-vectors, eq. (4) is actually relativistically covariant.

Because vorticity and circulation travel with the local flow velocity and are nonoscillatory in the local fluid frame, they have the potential to twist up and secularly amplify any magnetic field frozen into the flow. *A fundamental assumption of this paper is that the magnetic energy will eventually reach equipartition with the kinetic energy invested in the vortical part of the flow.* This assumption would also be well worth testing numerically.

For a general equation of state $P = P(\rho, N)$, where N is the proper number density of conserved particles (*e.g.*, baryons), it is conventional to take the quantity h in the relation $H^\mu = hU^\mu$ to be the enthalpy per particle: $h \equiv (\rho + P)/N$. One assumes an ideal fluid, so that the energy-momentum tensor is

$$T^{\mu\nu} \equiv (\rho + P)U^\mu U^\nu + Pg^{\mu\nu}, \quad (5)$$

($g^{\mu\nu} \rightarrow \text{diag}(-1, 1, 1, 1)$ in Minkowski coordinates), and the equations of motion are

$$T^{\mu\nu}_{;\nu} = 0 \quad \text{and} \quad (NU^\mu)_{;\mu} = 0. \quad (6)$$

The First Law of Thermodynamics $dh = TdS + N^{-1}dP$ implies $h_{,\mu} = P_{,\mu}/N$ if the fluid is isentropic; the first equation of motion in eq. (6) can then be recast as

$$U^\nu H^\mu_{;\nu} = -h_{,\mu}, \quad (7)$$

the “curl” of which implies eqs. (3) and (4) (*e.g.*, Eshraghi 2003, and Paper I). These relations do not hold across shocks, of course, since there is an entropy jump. But if the pre-shock medium is inhomogeneous, then even if the flow behind the shock is smooth, it will not be isentropic in general; that is, $P/N^{4/3}$ (for an ultra-relativistic equation of state) will not be uniform. Therefore, the conventional choice of h does not lead to a conserved circulation under the circumstances contemplated in this paper. Fortunately, as pointed out in Paper I, if one defines H^μ using $h \propto P^{1/4}$ instead of the true enthalpy, then eq. (7) always holds in smooth parts of the flow. This is a consequence of the equation of state $P = \rho/3$, which is “barytropic” if not isentropic. It is convenient to choose the constant of proportionality so that H^μ reduces to the fluid four-velocity when pressure is uniform. Therefore, we replace the conventional enthalpy current with

$$H^\mu \equiv (P/\bar{P})^{1/4} U^\mu. \quad (8)$$

With this choice, circulation is conserved [eqs. (3) & (4)] everywhere *except across shocks*.

2.2. Vorticity production by shocks

The goal of this subsection is to use the one-dimensional GSD approximation to derive eqs. (15)-(16), which relate the post-shock vorticity to the pre-shock fractional overdensity $\delta \equiv (\rho_0/\bar{\rho}_0) - 1$. Figure 1 illustrates four stages in the interaction of an ultra-relativistic shock with a density clump.

We begin by recalling some basic consequences of the shock jump conditions that will be needed below. Let $[Q]$ denote the discontinuity in a fluid property Q across the shock front. In

the instantaneous local rest frame of the shock, where the outward unit normal to the shock front is \mathbf{n} , the jump conditions are $[T^{\mu j} n_j] = 0$. Using eq. (5) for $T^{\mu\nu}$ (ideal fluid) and assuming that $P_0 \ll \rho_0$ ahead of the shock and $P = \rho/3$ behind it, one finds that the post-shock three-velocity of the fluid is $\mathbf{v} \cdot \mathbf{n} = -c/3$ in the shock frame (hence subsonic, since the sound speed is $c/\sqrt{3}$). The post-shock energy density is $\rho = 2\Gamma^2 \rho_0$, where $\Gamma \gg 1$ is the local Lorentz factor of the shock in the rest frame of the pre-shock fluid. Similarly, conservation of particles implies $[NU^i n_i] = 0$, whence $N = 2\sqrt{2}\Gamma N_0$. The quantities ρ , P , and N will always denote proper values, meaning that they are defined in the local fluid rest frame and are therefore Lorentz invariants by fiat, with subscript “0” denoting a pre-shock value rather than a spacetime index.

To facilitate Lorentz boosts between the pre-shock and post-shock or shock frames, it is often convenient to use the rapidity parameter $\tanh^{-1}(v/c)$, where v is the three-velocity in the pre-shock frame. The relativistic addition of colinear three-velocities is equivalent to addition of the corresponding rapidity parameters. Thus, for example, using $\Phi = \cosh^{-1} \Gamma \approx \ln(2\Gamma)$ for the rapidity parameter of the shock and ϕ for the rapidity of the post-shock fluid, it follows from the above that $\tanh(\phi - \Phi) = -1/3$, whence $\phi = \Phi - \ln \sqrt{2}$. The Lorentz factor of the post-shock fluid relative to the pre-shock frame is $\cosh \phi = \cosh(\Phi - \ln \sqrt{2}) = \Gamma/\sqrt{2} + O(\Gamma^{-1})$.

Pre-shock clumps will typically have comparable longitudinal and lateral dimensions (meaning: along and perpendicular to the *mean* direction of shock propagation) in their own rest frame. In the shock and post-shock frames, the clumps will be longitudinally contracted by factors $\sim \Gamma^{-1} \ll 1$. During the transit of the shock over a clump, and even during the subsequent expansion of the shocked clump as it comes to pressure equilibrium with the surrounding post-shock fluid, there will not be enough time for signals (sound waves) to communicate laterally from one end of the clump to the other. Therefore, the interaction of the shock with the clump can be calculated in a one-dimensional approximation, in which the area of the shock is constant and the pre-shock mass density (ρ_0/c^2) is stratified on planes parallel to the shock front.

Nevertheless, lateral density gradients do produce post-shock vorticity, $\boldsymbol{\omega}$, even in our one-dimensional approximation. First of all, the longitudinal component \mathbf{H}_{\parallel} of the non-conventional enthalpy current defined in eq. (8) varies with lateral position behind the shock. Secondly, since the shock itself is delayed differently at different lateral positions, the shock normal develops a lateral component, which leads to a small lateral current, \mathbf{H}_{\perp} . Although the magnitude of \mathbf{H}_{\perp} is $O(\Gamma^{-1})$ compared to \mathbf{H}_{\parallel} for a given clump amplitude, its longitudinal derivative makes a contribution to $\boldsymbol{\omega}$ that is comparable to the lateral derivative of \mathbf{H}_{\parallel} , as a consequence of Lorentz contraction.

Let $\delta(\mathbf{r})$ be the density contrast of the clump: $\rho_0(\mathbf{r}) = \bar{\rho}_0[1 + \delta(\mathbf{r})]$, where $\bar{\rho}_0$ is the mean pre-shock value. The shock propagates along z on average; let us choose a cartesian coordinate system x, y, z_0 in the pre-shock rest frame, where the subscript “0” is used to distinguish between the post-shock (z) and pre-shock (z_0) longitudinal coordinates. In our one-dimensional GSD approximation, it follows from eq. (1) that

$$\Gamma(\mathbf{r}) = \bar{\Gamma}[1 + \delta(\mathbf{r})]^{-\lambda}, \quad (9)$$

if $\bar{\Gamma} \gg 1$ is the value for a smooth pre-shock medium. As discussed at the beginning of this section, it will be assumed that $|\delta|^\lambda \ll \bar{\Gamma}$ so that $\Gamma \gg 1$ at all times; since $\lambda \approx 0.232$ is fairly small, rather hefty density contrasts can be compatible with this condition.

First of all, let us focus on the contribution of \mathbf{H}_\perp to the post-shock vorticity. Let $\tau(\mathbf{r})$ be the time in the pre-shock frame at which the shock reaches pre-shock position \mathbf{r} :

$$c\tau(x, y, z_0) \approx z_0 + \frac{1}{2}\bar{\Gamma}^{-2} \int_{-z_0}^{z_0} [1 + \delta(x, y, z'_0)]^{2\lambda} dz'_0 \equiv z_0 + \frac{1}{2}\bar{\Gamma}^{-2} I(x, y, z_0). \quad (10)$$

where we have assumed that the typical size of a density clump is small compared to the characteristic lengthscale for variations in $\bar{\Gamma}$. The shock surface at time t is determined implicitly by $\tau(\mathbf{r}) = t$, so that the shock normal is $\mathbf{n} = |\nabla_0 \tau|^{-1} \nabla_0 \tau$ (the subscript reminds that derivatives are taken ahead of the shock). To leading order in $\bar{\Gamma}^{-1}$, the lateral components of the normal are therefore

$$\mathbf{n}_\perp \approx \lambda \bar{\Gamma}^{-2} \nabla_\perp I = \lambda \bar{\Gamma}^{-2} \int_{-z_0}^{z_0} (1 + \delta')^{2\lambda-1} (\nabla_\perp \delta') dz'_0. \quad (11)$$

Here δ' is shorthand for $\delta(x, y, z'_0)$ and $\nabla_\perp \equiv (\partial/\partial x, \partial/\partial y, 0)$ is the same in the pre-shock and post-shock reference frames. The lateral part of the post-shock fluid 4-velocity is $\mathbf{U}_\perp \approx \mathbf{n}_\perp U_\parallel \approx \mathbf{n}_\perp \Gamma/\sqrt{2}$. With use of eqs. (8) and (9), the post-shock lateral enthalpy current becomes

$$\mathbf{H}_\perp \approx 2^{-1/2} \lambda \bar{\Gamma}^{-1} (1 + \delta)^{(1-6\lambda)/4} \nabla_\perp I. \quad (12)$$

Of course the lateral components of the enthalpy current take the same values in the mean post-shock and pre-shock frames since these frames differ by a longitudinal boost. However, in order to compute the vorticity in the mean post-shock fluid frame, we should remember that the longitudinal derivative in this reference system ∇_\parallel is related to the corresponding derivative $\nabla_{0,\parallel}$ in the pre-shock frame by $\nabla_\parallel = \cosh \bar{\phi} \nabla_{0,\parallel}$ because of Lorentz contraction. Thus the contribution of \mathbf{H}_\perp to the post-shock vorticity is

$$\begin{aligned} \nabla_\parallel \times \mathbf{H}_\perp &\approx \frac{1}{2} \lambda (1 + \delta)^{(2\lambda-3)/4} (\bar{\mathbf{n}} \times \nabla \delta) \\ &+ \frac{\lambda(1-6\lambda)}{8} (1 + \delta)^{-3(1+2\lambda)/4} \frac{\partial \delta}{\partial z_0} (\bar{\mathbf{n}} \times \nabla I) \end{aligned} \quad (13)$$

where $\bar{\mathbf{n}} = \mathbf{e}_z$ is the mean shock normal and clearly the differential operator $\bar{\mathbf{n}} \times \nabla$ is the same in the pre-shock and post-shock mean rest frames.

A comparable contribution to the post-shock vorticity comes from \mathbf{H}_\parallel . The longitudinal component of the post-shock 4-velocity is $\mathbf{U}_\parallel = \sinh(\phi - \bar{\phi}) \mathbf{e}_z$ when measured in the mean post-shock frame. Since $\phi - \bar{\phi} = \Phi - \bar{\Phi} = -\lambda \ln(1 + \delta)$,

$$\mathbf{U}_\parallel = -\frac{1}{2} \left[(1 + \delta)^\lambda - (1 + \delta)^{-\lambda} \right] \mathbf{e}_z \quad (14)$$

in the mean post-shock frame. This tends to be quite subluminal: for unit overdensity ($\delta = 1$), for example, $\mathbf{U}_\parallel \approx -0.1615 \mathbf{e}_z$, and the corresponding fluid Lorentz factor is ≈ 1.013 . The longitudinal

post-shock enthalpy current is $\mathbf{H}_{\parallel} = (P/\bar{P})^{1/4} \mathbf{U}_{\parallel} = (1+\delta)^{(1-2\lambda)/4} \mathbf{U}_{\parallel}$. Taking the lateral derivative of this and combining with eq. (13) and the definition of I in eq. (10), we can write the total post-shock vorticity as

$$\begin{aligned} \boldsymbol{\omega} \approx & c(\bar{\mathbf{n}} \times \nabla \delta) f(\delta) \\ & + c \frac{\lambda(1-6\lambda)}{8} (1+\delta)^{-3(1+2\lambda)/4} \frac{\partial \delta}{\partial z_0} \int_{z_0}^{z_0} (1+\delta')^{2\lambda-1} (\bar{\mathbf{n}} \times \nabla \delta') dz'_0, \end{aligned} \quad (15)$$

where the coordinate system is in the pre-shock rest frame and the derivatives are taken ahead of the shock. We have introduced the function

$$f(\delta) \equiv (1+\delta)^{-(2\lambda+3)/4} \left[\frac{6\lambda+1}{8} (1+\delta)^{\lambda} + \frac{6\lambda-1}{8} (1+\delta)^{-\lambda} \right]. \quad (16)$$

For $|\delta| \ll 1$, $f(\delta) \approx 3\lambda/2 \approx 0.348$. It is interesting that in the total post-shock vorticity there are no surviving factors of $\bar{\Gamma}$.

2.3. Vortical energy

We have not been able to formulate a rigorous relativistically covariant way of dividing the energy of the post-shock flow into vortical and non-vortical parts. In a non-relativistic flow, however, this would be straightforward. One would divide the three-velocity field into potential and solenoidal parts,

$$\mathbf{v} = \nabla \psi + \nabla \times \mathbf{A}, \quad (17)$$

and then define the vortical energy by

$$E_{\text{vort}} \equiv \frac{1}{2} \int \rho_m |\nabla \times \mathbf{A}|^2 d^3x, \quad (18)$$

where ρ_m is the non-relativistic mass density. To make the decomposition (17) unique, some mild additional restrictions are necessary: for example, that the region of interest is simply connected, and that ψ and \mathbf{A} have some specified behavior on the boundary or at infinity. Then one can impose $\nabla \cdot \mathbf{A} = 0$ and solve for \mathbf{A} from

$$\nabla^2 \mathbf{A} = -\boldsymbol{\omega}, \quad (19)$$

with $\boldsymbol{\omega} \equiv \nabla \times \mathbf{v}$, using an appropriate Green's function to invert ∇^2 . The nonvortical part follows similarly from $\nabla^2 \psi = \nabla \cdot \mathbf{v}$.

It isn't clear how to proceed in the relativistic case because the coordinate energy density T^{00} isn't simply quadratic in \mathbf{v} , in general. However, for the applications we have in mind, the vortical motions are plausibly subsonic in the mean post-shock frame (as long as δ is not too large), and therefore only mildly relativistic, $(v/c)^2 \lesssim 1/3$. Therefore, we will use the decomposition (17),

except for three changes: (i) $c\mathbf{H}$ replaces \mathbf{v} , and therefore $\boldsymbol{\omega} \rightarrow c\boldsymbol{\nabla} \times \mathbf{H}$ in eq. (19); (ii) ρ_m , the non-relativistic mass density, is replaced by ρ/c^2 , where ρ is the proper internal energy density; (iii) the factor 1/2 in eq. (17) is replaced by 4/3. The reason for (iii) is that if $v/c \ll 1$ and $P = \rho/3$, then $T^{00} \approx \rho + (4/3)\rho(v/c)^2$, and we assume that E_{vort} derives from the second term.¹

A pre-shock density clump will experience, after the transit across the shock front, a contraction of its longitudinal size by a factor α^{-1} , where $\alpha \equiv N/N_0 \approx 2\sqrt{2}\bar{\Gamma} \gg 1$. What was an approximately spherical clump becomes a pancake, with all of its associated vorticity in or near the interior. We adopt post-shock cylindrical coordinates R, θ, z with the z axis parallel to the mean direction of propagation of the shock. Taking the origin at the center of the clump, assuming the clump to be axisymmetric, and recalling that the vorticity computed in eq. (15) has been expressed in pre-shock coordinates, we may write $\boldsymbol{\omega} = \omega(R, z_0)\mathbf{e}_\theta = \omega(R, \alpha z)\mathbf{e}_\theta \approx \sigma(R)\delta_D(z)\mathbf{e}_\theta$, where $\delta_D(z)$ is the Dirac delta function, and

$$\sigma(R) \equiv \int_{-\infty}^{+\infty} \omega(R, \alpha z) dz = \frac{1}{\alpha} \int_{-\infty}^{+\infty} \omega(R, z_0) dz_0 \quad (20)$$

will be referred to as the “projected vorticity”.

Just after the shock passage, a clump will be at higher pressure than its surroundings, as already discussed, and will therefore expand until it reaches approximate pressure equilibrium. Since the sound-crossing time in the longitudinal direction will be much less than that in lateral directions, equilibrium will be reached with only a small fractional change in the lateral size. The fractional change in the longitudinal size will be of order unity, but for $\bar{\Gamma} \gg 1$ and clump overdensities $\delta \ll \bar{\Gamma}^{\gamma_{\text{ad}}/(1-2\lambda)}$ ($\gamma_{\text{ad}} = 2$ is the adiabatic index appropriate for the one-dimensional expansion of an ultra-relativistic fluid) the clump will remain highly flattened even after equilibration. Since the vortex lines lie parallel to the clump midplane (*i.e.*, in the direction \mathbf{e}_θ) and are “frozen” into the clump (as a consequence of Kelvin’s Circulation Theorem), the expansion will have little effect on the projected vorticity in eq. (20). We may therefore solve eq. (19) in the approximation that the vorticity is confined to a thin sheet with the projected vorticity computed in eq. (20). The problem is mathematically equivalent to finding the vector potential due to an axisymmetric current sheet carrying a toroidal current:

$$\mathbf{A}(R, z) = A(R, z)\mathbf{e}_\theta = \frac{1}{2} \int_0^{+\infty} \tilde{\sigma}(k) J_1(kR) e^{-k|z|} dk \mathbf{e}_\theta \quad (21)$$

¹Why 4/3 rather than 1/2, as one might expect in the non-relativistic limit? The answer is that the rest-mass density of non-relativistic fluid mechanics is actually $\rho_m = \gamma Nm$, where m is the mass per particle and $\gamma = U^0$, whereas the proper energy density is $\rho = Nm(c^2 + u)$, where mu is the internal energy per particle. Thus, for a general equation of state, $T^{00} = \gamma^2 \rho + (\gamma^2 - 1)P = \gamma \rho_m(c^2 + u) + (\gamma^2 - 1)P$. For $(v/c)^2 \ll 1$, this reduces to $T^{00} \approx \rho_m c^2 + \rho_m(v^2/2 + u) + [(v/c)^2(\rho_m u/2 + P)]$. The middle term is now recognizable as the non-relativistic kinetic-plus-internal energy density. The term in square brackets would normally be negligible for a cold fluid because $u \sim P/\rho_m \ll c^2$; however, for an ultra-relativistic ideal fluid $u \approx 3P\gamma/\rho_m \gg c^2$ and the result is $T^{00} \approx \rho_m c^2 + \rho_m v^2/2 + 3P + 4P(v/c)^2$, of which the first two terms are now negligible.

where $J_1(kR)$ is the Bessel function of order 1 and $\tilde{\sigma}(k)$ is the Hankel transform of the projected vorticity $\sigma(R)$:

$$\tilde{\sigma}(k) \equiv \int_0^{+\infty} \sigma(R) J_1(kR) R dR. \quad (22)$$

As soon as the clump is at the same pressure as its surroundings, if the vortical motions are sub-relativistic we can use the decomposition (17) with $\mathbf{v}_{\text{vort}} \rightarrow c \mathbf{H}_{\text{vort}} = \nabla \times \mathbf{A}$. Moreover, pressure equilibrium between the clump and the average post-shock medium implies² that the clump proper energy density ρ is approximately equal (neglecting terms of order $O(v^2/c^2)$) to the mean post-shock value $\bar{\rho}$. Then the vortical energy of a single clump becomes

$$E_{\text{vort}} \equiv \frac{4}{3} \bar{\rho} \int \frac{|\nabla \times \mathbf{A}|^2}{c^2} d^3x = -\frac{4}{3} \bar{\rho} \int \frac{\mathbf{A} \cdot \nabla^2 \mathbf{A}}{c^2} d^3x = \frac{4}{3} \bar{\rho} \int \frac{\mathbf{A} \cdot \boldsymbol{\omega}}{c^2} d^3x. \quad (23)$$

In accordance with the discussion following (19), we have replaced the factor $1/2$ in (18) with $4/3$. Also, we have used integration by parts to replace the integral over all space with an integral over the source of vorticity only. This is particularly convenient when the source is represented by a vortex sheet, because we may express the energy as an integral in k space:

$$E_{\text{vort}} = \frac{8\pi}{3} \bar{\rho} \int_0^{+\infty} \frac{A(R, 0) \sigma(R)}{c^2} R dR = \frac{4\pi}{3} \bar{\rho} \int_0^{+\infty} \frac{\tilde{\sigma}^2(k)}{c^2} dk. \quad (24)$$

We shall assume that the vortical energies of different clumps can simply be added. This is justified if the clumps are well separated compared to their larger (*i.e.*, lateral) dimensions. Then if the number density of clumps in the pre-shock frame is $N_{c,0}$ and all the clumps have the same axisymmetric density profile, the vortical energy density in the average post-shock frame is $\rho_{\text{vort}} = \alpha N_{c,0} E_{\text{vort}}$, and the vortical energy fraction becomes

$$\epsilon_{\text{vort}} \equiv \frac{\rho_{\text{vort}}}{\bar{\rho}} = \frac{4\pi}{3} \alpha N_{c,0} \int_0^{+\infty} \frac{\tilde{\sigma}^2(k)}{c^2} dk. \quad (25)$$

Recall from eq. (20) that the projected vorticity is proportional to $\alpha^{-1} = (2\sqrt{2}\bar{\Gamma})^{-1}$. Since this factor is squared in computing the vortical energy, it follows from eq. (25) that $\epsilon_{\text{vort}} \propto \bar{\Gamma}^{-1}$ for a fixed pre-shock density field. This scaling is perhaps the most important conclusion of our analysis up to this point.

²In the mean post-shock rest frame, if $T^{\mu\nu}$ is the energy-momentum tensor of the fluid in turbulent motion and $\bar{T}^{\mu\nu}$ for the mean fluid (whose four-velocity has spatial components $\bar{U}_i = 0$ in this reference frame), pressure equilibrium requires $T^{ij} = \bar{T}^{ij}$; under the assumption of spatial statistical isotropy for the turbulent motions, this implies $T^{kk} = 3\bar{P}$, which yields, for an ultra-relativistic fluid ($T^{\mu\mu} = \bar{T}^{\mu\mu} = 0$), the equality $T^{00} = \bar{\rho}$; then, since $T^{00} \approx \rho + (4/3)\rho(v/c)^2$, if the vortical motions are sub-relativistic we obtain $\rho \approx \bar{\rho}$.

3. The circumburst medium

Observations support the idea that long-duration GRBs are associated with the deaths of massive Wolf-Rayet (WR) stars, presumably arising from their core-collapse (Woosley & Bloom 2006, and references therein). Then the circumburst environment is determined by the star’s mass-loss history. At the onset of the WR phase, the WR stellar wind is expected to expand with a typical velocity $v_{\text{WR}} \approx 2000 \text{ km s}^{-1}$ inside the pre-existing slower wind emitted during the red supergiant (RSG) phase, whose characteristic speed is $v_{\text{RSG}} \approx 20 \text{ km s}^{-1}$. The winds from massive RSGs are characterized by a mass-loss rate \dot{M}_{RSG} between 10^{-6} and $10^{-4} \text{ M}_{\odot} \text{ yr}^{-1}$ (Chevalier et al. 2006), while the mass-loss rates \dot{M}_{WR} of WR stars are between 10^{-5} and $10^{-4} \text{ M}_{\odot} \text{ yr}^{-1}$ (Crowther 2006). Several solar masses are shed by the star during these evolutionary phases. The mass equivalent to the energy of a GRB, on the other hand, is only $\approx 0.06 E_{\text{iso},53} \text{ M}_{\odot}$. Therefore, the GRB forward shock is expected to become non-relativistic long before it escapes the wind to encounter the interstellar medium. There are at least four regions of the wind that are relevant to the relativistic phase of the afterglow (Ramirez-Ruiz et al. 2005): from the inside out, these are an expanding WR wind ($\bar{\rho}_0/c^2 = \dot{M}_{\text{WR}}/4\pi v_{\text{WR}} r^2$, where r is the distance from the star), the shocked WR wind ($\bar{\rho}_0 \approx \text{constant}$), the shocked RSG wind ($\bar{\rho}_0 \approx \text{constant}$), and a freely expanding RSG wind ($\bar{\rho}_0/c^2 = \dot{M}_{\text{RSG}}/4\pi v_{\text{RSG}} r^2$). Beyond these lie another shocked part of the RSG wind, the shocked ISM, and finally the unshocked ISM.

Density inhomogeneities in such a stratified structure could be produced by several processes. First of all, the acceleration region of the WR wind, which extends to a few times the stellar radius, is known to be clumpy. Emission-line data indicate accelerating “blobs” (Moffat et al. 1988) with density filling factors $f \approx 0.05 - 0.25$ (Crowther 2006, and references therein). These must occur where the continuum is optically thin and must be large enough transversely to cover an appreciable part ($\gtrsim 10\%$) of the stellar photosphere. The clumpiness of this region is in accord with theory, since the line-driving mechanism of Castor et al. (1975), which explains the gross properties of WR and main-sequence O-star winds rather satisfactorily, is known to be unstable both radially and nonradially on scales larger than the “Sobolev length” $l_{\text{Sob}} \sim r v_{\text{th}}/v_{\text{WR}} \approx 10^{-2} r$ (Dessart & Owocki 2005, and references therein), where $v_{\text{th}} \approx 20 \text{ km s}^{-1}$ is the thermal velocity in the wind. Clump dimensions at least as small as $\sim 10^{10} \text{ cm}$ with density contrasts $\sim f^{-1} \sim 10$ are therefore expected. These clumps may dissolve beyond the acceleration region ($r \gg 10^{12} \text{ cm}$) if the optically thin wind maintains a uniform temperature comparable to the color temperature of the star; the clumps are then at higher density than their surroundings and will expand on their sound-crossing time. After crossing the reverse shock, the wind reaches temperatures $\sim 10^8 \text{ K}$, a regime that is thermally unstable (Field 1965). Beyond the contact discontinuity, the shocked RSG wind lies at $T \sim 10^6 \text{ K}$, which is even more unstable. Thermal instability may give rise to new clumps, whose minimum size is controlled by thermal conduction and is therefore very uncertain because the conduction rate is probably sensitive to magnetic field. Furthermore, the contact discontinuity is subject to Rayleigh-Taylor instability as the shocked RSG wind is accelerated by the less dense WR wind; however, Garcia-Segura & Franco (1996) found that clump formation is not efficient for the case of

pure Rayleigh-Taylor instabilities in thick shells and concluded that a necessary condition for clump development to occur is that the shocked shell be thin enough to allow Vishniac-like instabilities (Vishniac 1983). Ramirez-Ruiz et al. (2005) point out that rapid cooling of the shocked RSG wind is indeed likely to lead to a thin shell. Clump development in the shell is controlled by the Kelvin-Helmholtz damping of the coupling between the Rayleigh-Taylor and Vishniac instabilities, while the lifetime of small dense clumps, once formed, probably again depends upon conduction.

In short, there are ample reasons to expect a strongly inhomogeneous medium ahead of the GRB forward shock, but the sizes of the smallest clumps are uncertain. We make no attempt to estimate these sizes but simply state below the properties (lengthscale, density contrast and number density) that the clumps would have to have in order to produce post-shock turbulence capable of amplifying the magnetic field sufficiently.

It is of course essential for our proposed mechanism that a seed field exist in the pre-shock medium. Magnetic and thermal energy densities are generally comparable in the ISM, but much less is known about the magnetic component of the winds of early-type stars. Since such winds are believed to be driven by radiative rather than centrifugal forces, as in late-type main-sequence stars, and since such stars do not possess surface convection zones, the magnetic field might be very small *a priori*. However, magnetic effects have been invoked to explain X-ray emission and anisotropy in the winds of early-type stars (Wolf et al. 1999; ud-Doula & Owocki 2002; Schulz et al. 2003). Furthermore, since the amplification of a weak (kinematic) magnetic energy density by turbulence proceeds exponentially on the timescale of the energy-bearing eddies (Schekochihin et al. 2002, and references therein), the number N_{eddy} of eddy-turnover times required to reach saturation is only logarithmically dependent on the strength of the seed field. Therefore, in the estimates of the required turnover time made below, we shall simply assume that the magnetic energy fraction ϵ_B in the pre-shock medium is comparable to that in the ISM, $\sim 10^{-8}$, so that the number of eddy rotations necessary to explain the value of ϵ_B inferred from afterglow observations is of order $N_{\text{eddy}} \sim 10$.

4. Results

The formalism described in §II can be used to predict the eddy-turnover time and vortical energy fraction of the turbulent motions produced by an ultra-relativistic shock sweeping-up a clumpy medium; if the pre-shock average (*i.e.*, smoothed over clumps) density profile is known, a comparison with afterglow models will then let us constrain the lengthscale, overdensity and volume filling factor of the circumburst inhomogeneities. Unfortunately, observations have not yet clearly determined the density profile ahead of the GRB forward shock (Chevalier & Li 2000; Panaitescu & Kumar 2001, 2002; Chevalier et al. 2004), so that we will consider both free winds (energy density $\bar{\rho}_0 \propto r^{-2}$) and shocked uniform winds ($\bar{\rho}_0 \approx \text{constant}$) as possible circumburst media, keeping in mind that, as described by Ramirez-Ruiz et al. (2005) and outlined in §III, the actual surrounding environment is much more complex.

Assuming that the blast wave is adiabatic and effectively spherical and that $E_{\text{iso}} = 10^{53} E_{\text{iso},53}$ erg is its isotropic equivalent energy, as derived from the gamma-ray output, we can compute the deceleration radius of the GRB forward shock when about half of the initial energy has been transferred to the shocked matter; for an initial Lorentz factor $\Gamma_0 = 10^2 \Gamma_{0,2}$, the typical swept-up mass where this happens is

$$M_{\text{dec}} = \frac{E_{\text{iso}}}{\Gamma_0^2 c^2} \approx 5.6 \times 10^{-6} E_{\text{iso},53} \Gamma_{0,2}^{-2} M_{\odot}. \quad (26)$$

For the two circumburst density profiles mentioned above, the deceleration radius of the shock is then

$$r_{\text{dec}} = \begin{cases} \frac{M_{\text{dec}} v_{\text{WR}}}{\dot{M}_{\text{WR}}} \approx 3.5 \times 10^{15} E_{\text{iso},53} v_{\text{WR},8.3} \dot{M}_{\text{WR},-5}^{-1} \Gamma_{0,2}^{-2} \text{ cm} & \text{for } \bar{\rho}_0 \propto r^{-2} \\ \left(\frac{3 M_{\text{dec}}}{4\pi m_p n_{\text{ISM}}} \right)^{1/3} \approx 1.2 \times 10^{17} (E_{\text{iso},53}/n_{\text{ISM},0})^{1/3} \Gamma_{0,2}^{-2/3} \text{ cm} & \text{for } \bar{\rho}_0 \approx \text{const.} \end{cases} \quad (27)$$

where in the first case we have chosen typical WR wind parameters ($\dot{M}_{\text{WR}} = 10^{-5} \dot{M}_{\text{WR},-5} M_{\odot} \text{yr}^{-1}$ and $v_{\text{WR}} = 2000 v_{\text{WR},8.3} \text{ km s}^{-1}$), whereas in the second case a baryon number density comparable to the ISM value ($n_{\text{ISM}} = n_{\text{ISM},0} \text{ cm}^{-3}$) has been assumed. This corresponds to a deceleration time in the post-shock rest frame

$$t_{\text{dec}} = \sqrt{2} \frac{r_{\text{dec}}}{\Gamma_0 c} \approx \begin{cases} 1.7 \times 10^3 E_{\text{iso},53} v_{\text{WR},8.3} \dot{M}_{\text{WR},-5}^{-1} \Gamma_{0,2}^{-3} \text{ s} & \text{for } \bar{\rho}_0 \propto r^{-2} \\ 5.7 \times 10^4 (E_{\text{iso},53}/n_{\text{ISM},0})^{1/3} \Gamma_{0,2}^{-5/3} \text{ s} & \text{for } \bar{\rho}_0 \approx \text{const.} \end{cases} \quad (28)$$

since the Lorentz factor of the post-shock material in the pre-shock rest frame is $\Gamma_0/\sqrt{2}$.

4.1. Clump properties

We consider a pre-shock medium with number density $N_{\text{c},0}$ of identical clumps. Each clump is characterized by a gaussian overdensity profile with central density contrast δ_{max} and typical size L ; if the origin of the axes is in the center of the clump and R , z_0 and θ are pre-shock cylindrical coordinates, we choose a clump energy density profile

$$\rho_0(R, z_0) = \rho_{\text{ext}} [1 + \delta_{\text{max}} e^{-(R^2 + z_0^2)/L^2}] , \quad (29)$$

where ρ_{ext} is the energy density of the inter-clump homogeneous medium. In order to use the formalism introduced in §II—where the density contrast δ was defined with respect to the mean pre-shock energy density $\bar{\rho}_0$ (averaged over clumps), whereas here the inter-clump density ρ_{ext} has been used—we should set

$$\delta(R, z_0) = \frac{\rho_{\text{ext}}}{\bar{\rho}_0} [1 + \delta_{\text{max}} e^{-(R^2 + z_0^2)/L^2}] - 1 ; \quad (30)$$

however, the ratio between ρ_{ext} and $\bar{\rho}_0$ can be easily computed for the density profile in eq. (29):

$$\frac{\rho_{\text{ext}}}{\bar{\rho}_0} = \frac{1}{1 + \pi^{3/2} \delta_{\text{max}} N_{\text{c},0} L^3} \approx 1 \quad (31)$$

provided that $\delta_{\max} N_{c,0} L^3 \lesssim 1$. In this section, we will always assume $\rho_{\text{ext}}/\bar{\rho}_0 \approx 1$, so that the formulae in §II can be used with a pre-shock overdensity profile

$$\delta(R, z_0) = \delta_{\max} e^{-(R^2 + z_0^2)/L^2}. \quad (32)$$

For small density contrasts, we can perform analytical calculations taking into account just the leading (first) order term in δ within eq. (15); the corresponding vorticity will be referred to as the “leading-order vorticity” ω_{LO} , and the Hankel transform of its projected vorticity will be used in eq. (25) to analytically compute the leading (second) order in δ_{\max} of the vortical energy fraction ($\epsilon_{\text{vort,LO}}$). This approximation is certainly well justified for $\delta_{\max} \ll 1$, but Figure 2 shows that the full numerical computation for ϵ_{vort} is still in reasonable agreement with our analytical approximation $\epsilon_{\text{vort,LO}}$ even for $\delta_{\max} \sim 1$. For larger central overdensities a numerical calculation is required, and we could fit the numerical results with a fitting function

$$\epsilon_{\text{vort}} = \epsilon_{\text{vort,LO}} \frac{1}{1 + c_1 (\delta_{\max})^{c_2}} \quad (33)$$

(c_1 and c_2 are fitting parameters), so that for small overdensities ($\delta_{\max} \ll 1$) we recover the result of the analytical computation.

4.2. Eddy-turnover time

Vorticity embedded in clumps by the passage of the GRB forward shock can be responsible for the magnetic fraction inferred from afterglow models only if vortical motions are fast and energetic enough to amplify the field up to the observed value before the shock deceleration time, when adiabatic expansion would significantly reduce the particle energies available for the afterglow emission.

In the leading-order approximation described above, an estimate of the eddy-turnover time for the density contrast in eq. (32) is

$$t_{\text{eddy}} = \frac{1}{|\omega_{\text{LO}}(L, 0)|} \approx 6.5 \times 10^2 L_{13} \frac{2}{\delta_{\max}} \text{ s} \quad (34)$$

where $L = 10^{13} L_{13}$ cm; the reference value chosen for the central overdensity δ_{\max} is in agreement with observations (see §III) and reasonably satisfies the requirements for the leading-order approximation (see Figure 2). If $N_{\text{eddy}} = 10 N_{\text{eddy},1}$ is the number of eddy rotations necessary to explain the observed ϵ_B , the requirement $N_{\text{eddy}} t_{\text{eddy}} \leq t_{\text{dec}}$ for a wind-like or ISM-like circumburst medium gives respectively

$$\begin{cases} L_{13} \frac{2}{\delta_{\max}} \lesssim 0.3 E_{\text{iso},53} v_{\text{WR},8.3} \dot{M}_{\text{WR},-5}^{-1} \Gamma_{0,2}^{-3} N_{\text{eddy},1}^{-1} & \text{for } \bar{\rho}_0 \propto r^{-2} \\ L_{13} \frac{2}{\delta_{\max}} \lesssim 8.7 (E_{\text{iso},53}/n_{\text{ISM},0})^{1/3} \Gamma_{0,2}^{-5/3} N_{\text{eddy},1}^{-1} & \text{for } \bar{\rho}_0 \approx \text{const.} \end{cases} \quad (35)$$

Let us emphasize that, for smaller initial shock Lorentz factors Γ_0 , a larger size L and weaker overdensity δ_{\max} are enough to satisfy the constraint $N_{\text{eddy}} t_{\text{eddy}} \leq t_{\text{dec}}$.

4.3. Vortical energy fraction

The kinetic energy density invested in the vortical part of the post-shock flow should be a significant fraction of its proper energy density, since—as stated in §II—we assume that the amplified magnetic fraction, which is required to match the observational inference $\epsilon_B \gtrsim 10^{-3}$, will eventually be comparable to the vortical fraction, $\epsilon_B \sim \epsilon_{\text{vort}}$. However, ϵ_B might be smaller than ϵ_{vort} if the backreaction of magnetic field on turbulent motions is important well before equipartition between the magnetic and vortical energy densities; on the other hand, ϵ_{vort} may also be a lower limit for ϵ_B if secondary shocks created by the overlapping sound waves of many different overpressured clumps significantly contribute to magnetic field amplification.

The results of a numerical calculation for the vortical fraction of clumps with overdensity profile in eq. (32) are shown in Figure 3 (*solid line*), but for small central overdensities the leading-order analytical computation described above gives a reliable estimate of the magnetic energy fraction produced by turbulence in GRB afterglows:

$$\epsilon_B \sim \epsilon_{\text{vort,LO}} \approx 1.8 \times 10^{-3} \bar{\Gamma}_2^{-1} \left(\frac{\delta_{\text{max}}}{2} \right)^2 \frac{N_{\text{c},0} L^3}{0.25} \quad (36)$$

where $\bar{\Gamma} = 10^2 \bar{\Gamma}_2$ and the reference values for the central overdensity δ_{max} and the clump volume filling factor $N_{\text{c},0} L^3$ have been chosen in order to match the observational constraint $\epsilon_B \gtrsim 10^{-3}$. So, clumps with moderate density contrasts ($\delta_{\text{max}} \approx 2$, in agreement with the observational evidences reviewed in §III) can justify the lower limit of the magnetic energy fraction inferred from afterglow models. Higher density contrasts (see Figure 3) would be necessary to achieve larger magnetic fractions; however, it is worth recalling that our model is applicable only under the assumptions that the clump overdensity is not larger than $\sim \Gamma$ (see §II) and that $\delta_{\text{max}} N_{\text{c},0} L^3 \lesssim 1$, so that the overdensity profile can actually be described by eq. (32).

Eq. (36) suggests that smaller overdensities would be enough to satisfy the observational constraints on ϵ_B as the forward shock slows down, since $\epsilon_B \propto \bar{\Gamma}^{-1}$; the magnetic fraction is then expected to change during the afterglow stage, and in §V we will discuss the possible observational consequences of its time evolution.

5. Summary and Discussion

We have proposed that the post-shock magnetic fields of GRB afterglows may arise from macroscopic MHD turbulence rather than microscopic plasma instabilities. The source of turbulence is vorticity produced when the shock encounters density inhomogeneities in the pre-shock medium. We presume that the magnetic energy fraction (ϵ_B) that results is comparable to the energy fraction of the turbulence. The ultra-relativistic Geometrical Shock Dynamics formalism of Paper I (Goodman & MacFadyen 2007) allows an easy, though approximate, calculation of the vorticity produced by a given density inhomogeneity in the limit that the shock Lorentz factor $\Gamma \gg 1$.

In this picture, the observational inference that $\epsilon_B \gtrsim 10^{-3}$ constrains both the amplitude and the lengthscale of inhomogeneities. Eqs. (33) and (36) roughly relate the total energy fraction in vortical motions to the volume filling factor and density contrast of the clumps; this energy fraction must be comparable to the inferred post-shock ϵ_B . Filling factors and density contrasts of order unity are required when the shock is still highly relativistic. Eq. (35), on the other hand, express the constraint on the lengthscale and density contrast of individual clumps (independently of their volume filling factor) so that the eddies can wind the magnetic field up to the observed value in less than the expansion time of the shock. This second constraint favors small lengthscales, so that the clumps responsible for field amplification would probably be too small, at least individually, to modulate the afterglow light curve. Actually, Nakar & Granot (2006) have recently shown that any pre-shock inhomogeneity can hardly be responsible for the rebrightenings observed in some afterglow light curves.

There is a question whether a fluid treatment of the post-shock flow is justified at all since the plasma is collisionless. The same question arises in supernova remnants, to which the standard answer is that magnetization of the plasma ensures a short effective mean free path. The present case is more extreme because the particles are relativistic, the lengthscales on which fluid-like behavior is required are smaller, especially in the present work, and the pre-shock field is energetically negligible. The relativistic Larmor radius of the post-shock ions based on the compressed ambient field is $r_L \approx \Gamma m_p c^2 / eB \approx 10^{12} (3 \mu\text{G} / B_0) \text{ cm}$, where B_0 is the pre-shock field strength. This is smaller than the maximum tolerable clump size for field amplification at the beginning of the afterglow phase, though only barely so (§4.2). Furthermore, whether or not the Weibel instability can produce persistent magnetic fields, it should enforce fluid-like behavior by isotropizing particle distribution functions whenever counterstreaming plasmas overlap.

A basic conclusion of this work is that vortical turbulence becomes easier to produce with decreasing shock Lorentz factor. Both the energy and timescale constraints become easier to satisfy as Γ decreases (however, our ultra-relativistic approximations break down as $\Gamma \rightarrow 1$). Therefore, if the post-shock magnetic energy density is produced by macroscopic turbulence, it is likely that ϵ_B will evolve as the shock ages, complicating the task of drawing physical inferences about the GRB environment from the observational data. The abundance of early X-ray light curves provided by the *Swift* satellite has already led to models that are more complicated than the rather simple theoretical description of the sparser *BeppoSAX* results (Galama et al. 1998). The light curves are not single power laws in time, but show breaks and sometimes “flares”, suggesting a need for extended energy input from the central source (Zhang et al. 2006, and references therein). But, to date, most modelers have assumed constant ϵ_B and ϵ_e (the post-shock energy fraction in relativistic e^\pm) within individual afterglows, although these parameters are often allowed to vary from one afterglow to another.

The effect of an evolving ϵ_B depends upon the relationship between the observed frequency and certain critical frequencies in the synchrotron spectrum. Particularly important is the cooling frequency, the doppler-shifted synchrotron frequency of a post-shock electron or positron that

radiates much of its energy on a timescale comparable to the age of the shock. For a pre-shock medium with mass density profile $\bar{\rho}_m(r) \equiv c^{-2}\bar{\rho}_0(r) = Kr^{-\omega}$ averaged over clumps, and for an adiabatic relativistic shock with constant isotropically equivalent energy E_{iso} (notwithstanding the above-cited inferences from *Swift* data), the cooling frequency evolves as (up to dimensionless constants of order unity)

$$\begin{aligned}\nu_{\text{cool}} &\approx \frac{e m_e}{(1 + z_{\text{GRB}}) \sigma_{\text{T}}^2} [\epsilon_{\text{B}} \bar{\rho}_m(r_s)]^{-3/2} r_s^{-2} \\ &\approx \frac{e m_e}{(1 + z_{\text{GRB}}) \sigma_{\text{T}}^2} \epsilon_{\text{B}}^{-3/2} K^{-4/(4-\omega)} \left[\frac{E_{\text{iso}}}{c} (1 + z_{\text{GRB}})^{-1} t \right]^{(3\omega-4)/2(4-\omega)},\end{aligned}\quad (37)$$

where r_s is the shock radius, t the astronomical observer's time and z_{GRB} the GRB cosmological redshift. Evidently, the shock energy and Lorentz factor scale out of the cooling frequency when the latter is expressed in terms of the shock radius. If one could be confident that the early afterglow evolves in a freely expanding wind ($\omega = 2$), which seems *a priori* likely in collapsar models, then the evolution of ϵ_{B} could be inferred by measuring that of ν_{cool} .

Present evidence suggests that the cooling frequency lies below the X-ray regime in the early afterglow phase. This conclusion rests on the usual assumption that the synchrotron-emitting electrons are injected with a power law distribution of energies, $N(\gamma)d\gamma \propto \gamma^{-p}d\gamma$ for $\gamma > \gamma_{\text{min}} \gg 1$, in which $p > 2$ so that the total energy is dominated by electron energies near $\gamma_{\text{min}} m_e c^2$, whose characteristic observed frequency is ν_{min} . The observed specific flux is often described as a power law in time and frequency, $F_\nu \propto t^{-\alpha} \nu^{-\beta}$, despite various breaks and the aforementioned flares. If synchrotron emission dominates and $\nu_{\text{cool}} > \nu_{\text{min}}$ (slow-cooling regime), the spectral index is $\beta = (p-1)/2$ if $\nu_{\text{min}} < \nu < \nu_{\text{cool}}$ and $\beta = p/2$ if $\nu > \nu_{\text{cool}}$. It is believed that the acceleration index p is not much larger than 2, perhaps $p \approx 2.2 - 2.3$, which is then consistent with the observed X-ray indices $\beta \approx -1$ observed by *Swift* (Zhang et al. 2006, and references therein) only if $h\nu_{\text{cool}} < 1$ keV. Evaluating eq. (37) at the deceleration radius appropriate for a Wolf-Rayet wind (see eq. (27)), we find that the afterglow phase begins with a cooling frequency that is plausibly consistent with this constraint:

$$h\nu_{\text{cool,dec}} \approx 0.2 (1 + z_{\text{GRB}})^{-1} (10^4 \epsilon_{\text{B}})^{-3/2} v_{\text{WR},8.3}^{5/2} \dot{M}_{\text{WR},-5}^{-5/2} E_{\text{iso},53} \Gamma_{0,2}^{-2} \text{ keV}. \quad (38)$$

Unless the cooling frequency passes through the observed band, one cannot learn much about the evolution of ϵ_{B} from observations at $\nu > \nu_{\text{cool}} > \nu_{\text{min}}$, because (up to numerical factors of order unity)

$$\nu F_\nu \approx \frac{\epsilon_e E_{\text{iso}}}{4\pi d_L^2 (1 + z_{\text{GRB}})^{-1} t} \left(\frac{\gamma}{\gamma_{\text{min}}} \right)^{2-p} \quad (39)$$

in this regime, where d_L is the luminosity distance; ϵ_{B} enters the above expression only *via* the correspondence $\nu \approx (1 + z_{\text{GRB}})^{-1} (\gamma \Gamma)^2 (\epsilon_{\text{B}} \bar{\rho}_m)^{1/2} e/m_e$ between observed frequency ν and electron Lorentz factor γ , and hence is raised to the small exponent $(p-2)/4 \lesssim 0.1$. On the other hand, relation (39) indicates that the flux above the cooling frequency provides an excellent measure of the energy in the electron population (Freedman & Waxman 2001).

We thank Ed Jenkins and Bruce Draine for discussions of small-scale inhomogeneities in the ISM, and Eli Waxman for discussions of recent GRB afterglow observations and their implications. This work was supported in part by the NSF Center for Magnetic Self-Organization at Princeton.

REFERENCES

- Castor, J. I., Abbott, D. C., & Klein, R. I. 1975, *ApJ*, 195, 157
- Chevalier, R. A., Fransson, C., & Nymark, T. K. 2006, *ApJ*, 641, 1029
- Chevalier, R. A., & Li, Z.-Y. 2000, *ApJ*, 536, 195
- Chevalier, R. A., Li, Z.-Y., & Fransson, C. 2004, *ApJ*, 606, 369
- Coburn, W., & Boggs, S. E. 2003, *Nature*, 423, 415
- Crowther, P. A. 2006, *ArXiv Astrophysics e-prints*
- Dessart, L., & Owocki, S. P. 2005, *A&A*, 437, 657
- Eshraghi, H. 2003, *Physics of Plasmas*, 10, 3577
- Field, G. B. 1965, *ApJ*, 142, 531
- Frederiksen, J. T., Hededal, C. B., Haugbølle, T., & Nordlund, Å. 2004, *ApJ*, 608, L13
- Freedman, D. L., & Waxman, E. 2001, *Astrophys. J.*, 547, 922
- Galama, T. J., Wijers, R. A. M. J., Bremer, M., Groot, P. J., Strom, R. G., Kouveliotou, C., & van Paradijs, J. 1998, *ApJ*, 500, L97+
- Garcia-Segura, G., & Franco, J. 1996, *ApJ*, 469, 171
- Genet, F., Daigne, F., & Mochkovitch, R. 2007, *ArXiv Astrophysics e-prints*
- Goodman, J., & MacFadyen, A. 2007, *J. Fluid. Mech.*, submitted (Paper I)
- Ishizuka, T., Hashimoto, Y., & Ōno, Y. 1964, *Progress of Theoretical Physics*, 32, 207
- Lazzati, D., Rossi, E., Covino, S., Ghisellini, G., & Malesani, D. 2002, *A&A*, 396, L5
- Medvedev, M. V., & Loeb, A. 1999, *ApJ*, 526, 697
- Meszáros, P., & Rees, M. J. 1997, *ApJ*, 476, 232
- Moffat, A. F. J., Drissen, L., Lamontagne, R., & Robert, C. 1988, *ApJ*, 334, 1038
- Nakar, E., & Granot, J. 2006, *ArXiv Astrophysics e-prints*
- Nakar, E., Piran, T., & Granot, J. 2003, *New Astronomy*, 8, 495
- Panaiteanu, A. 2005, *MNRAS*, 363, 1409
- Panaiteanu, A., & Kumar, P. 2001, *ApJ*, 554, 667

- . 2002, *ApJ*, 571, 779
- Ramirez-Ruiz, E., García-Segura, G., Salmonson, J. D., & Pérez-Rendón, B. 2005, *ApJ*, 631, 435
- Sari, R. 2006, *Physics of Fluids*, 18, 027106
- Schaefer, B. E., Gerardy, C. L., Höflich, P., Panaitescu, A., Quimby, R., Mader, J., Hill, G. J., Kumar, P., Wheeler, J. C., Eracleous, M., Sigurdsson, S., Mészáros, P., Zhang, B., Wang, L., Hessman, F. V., & Petrosian, V. 2003, *ApJ*, 588, 387
- Schekochihin, A. A., Cowley, S. C., Hammett, G. W., Maron, J. L., & McWilliams, J. C. 2002, *New Journal of Physics*, 4, 84
- Schulz, N. S., Canizares, C., Huenemoerder, D., & Tibbets, K. 2003, *ApJ*, 595, 365
- Silva, L. O., Fonseca, R. A., Tonge, J. W., Dawson, J. M., Mori, W. B., & Medvedev, M. V. 2003, *ApJ*, 596, L121
- Spitkovsky, A. 2005, in *AIP Conf. Proc. 801: Astrophysical Sources of High Energy Particles and Radiation*, ed. T. Bulik, B. Rudak, & G. Madejski, 345–350
- ud-Doula, A., & Owocki, S. P. 2002, *ApJ*, 576, 413
- Uhm, Z. L., & Beloborodov, A. M. 2007, *ArXiv Astrophysics e-prints*
- Vishniac, E. T. 1983, *ApJ*, 274, 152
- Völk, H. J., Berezhko, E. G., & Ksenofontov, L. T. 2005, *A&A*, 433, 229
- Wang, X., & Loeb, A. 2000, *ApJ*, 535, 788
- Waxman, E. 2006, *Plasma Physics and Controlled Fusion*, 48, B137
- Whitham, G. B. 1974, *Linear and Nonlinear Waves* (Wiley)
- Wolf, B., Stahl, O., & Fullerton, A. W., eds. 1999, *Variable and Non-spherical Stellar Winds in Luminous Hot Stars*
- Woosley, S. E., & Bloom, J. S. 2006, *ARA&A*, 44, 507
- Yost, S. A., Harrison, F. A., Sari, R., & Frail, D. A. 2003, *ApJ*, 597, 459
- Zhang, B., Fan, Y. Z., Dyks, J., Kobayashi, S., Mészáros, P., Burrows, D. N., Nousek, J. A., & Gehrels, N. 2006, *ApJ*, 642, 354
- Zhang, B., Kobayashi, S., & Mészáros, P. 2003, *ApJ*, 595, 950

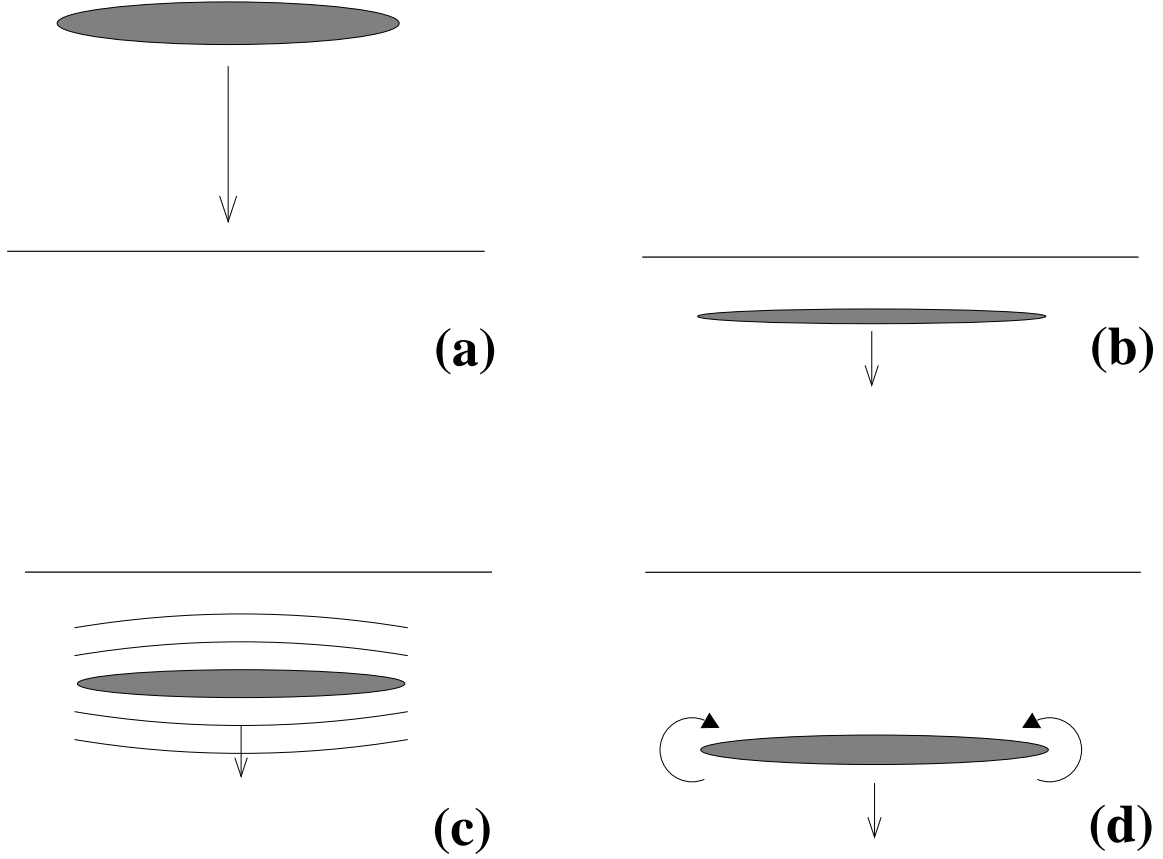


Fig. 1.— History of a density clump overrun by an ultra-relativistic shock (mean Lorentz factor $\bar{\Gamma}$), viewed in the shock rest frame. (a) The Lorentz-contracted (by a factor $\sim \bar{\Gamma}^{-1}$) spherical clump approaches the shock (thick line) with $v \approx c$. (b) After the shock, the clump contracts further by $\times 1/3$ (or $\times (2\sqrt{2})^{-1}$ in its rest frame) and moves downstream at $c/3$. (c) The clump re-expands to reach pressure equilibrium and emits sound waves or weak shocks. (d) Vorticity created by the shock passage begins to roll up the clump.

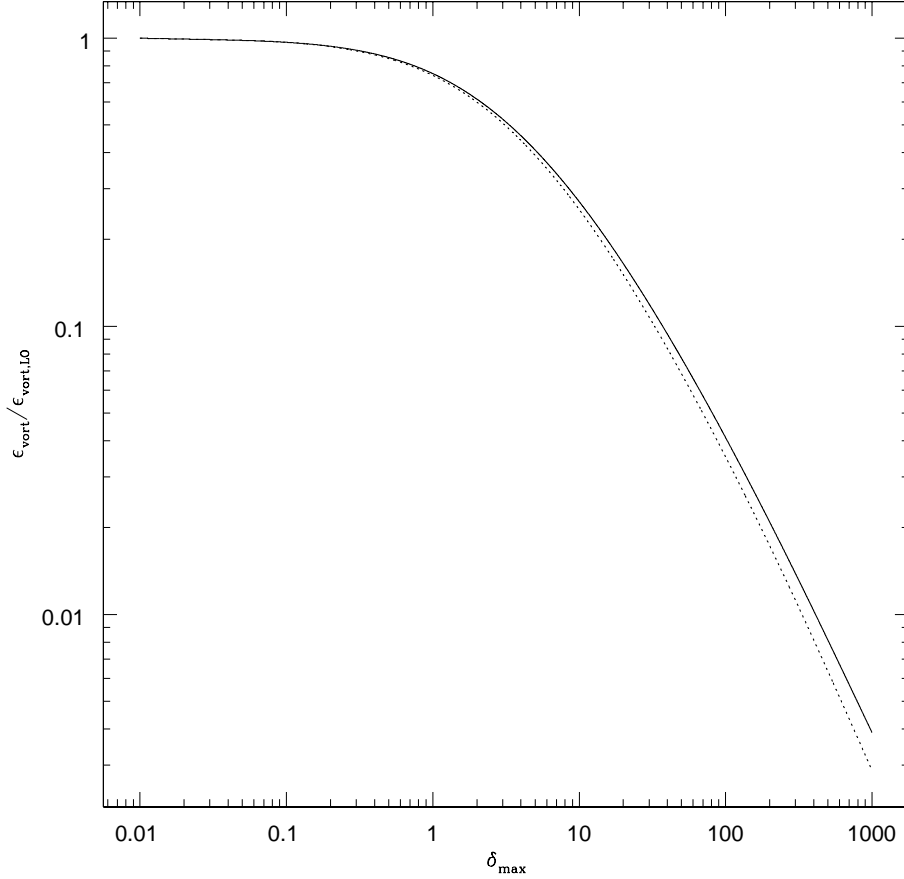


Fig. 2.— Ratio between the exact numerical calculation of the vortical energy fraction (ϵ_{vort}) and its analytical approximation ($\epsilon_{\text{vort,LO}}$ in eq. (36), keeping only the leading order in the central overdensity δ_{max} within the vorticity ω) as a function of δ_{max} ; deviations from the analytical calculation are significant only for $\delta_{\text{max}} \gtrsim 1$. *Dotted line*: Taking into account, in the numerical calculation, only the non-integral contribution to the vorticity (*i.e.*, neglecting the second row in eq. (15)). *Solid line*: Full numerical calculation, including both the integral and non-integral terms in eq. (15); the non-integral contribution is found to be dominant even for large overdensities.

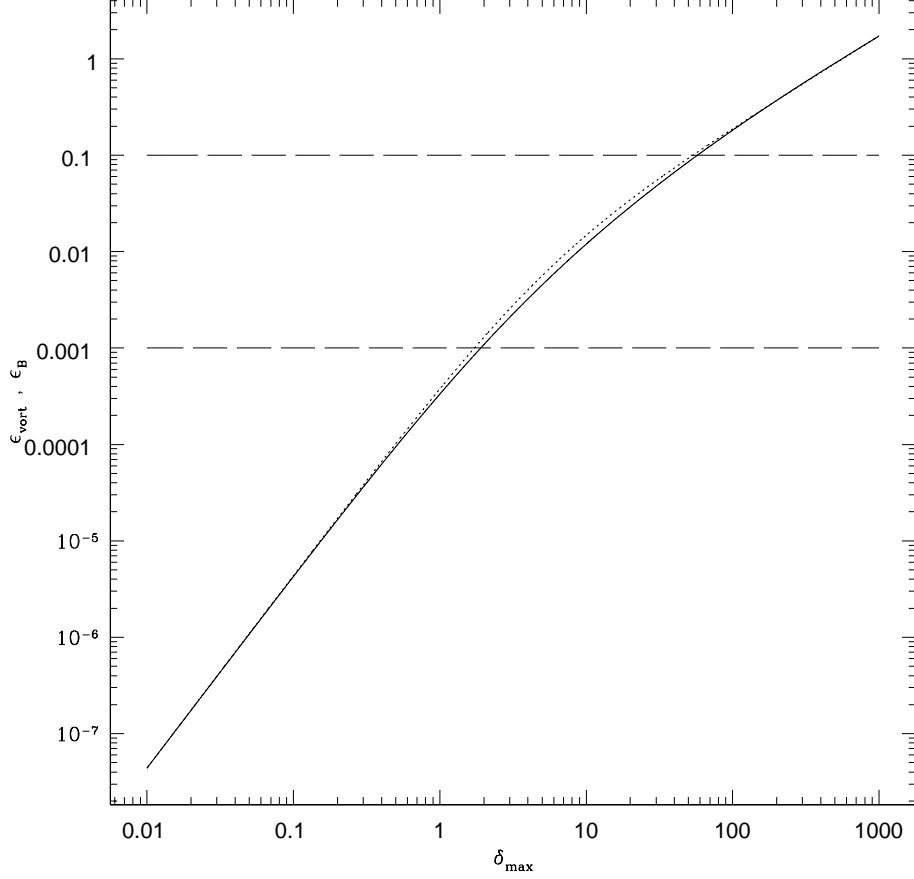


Fig. 3.— *Solid line*: Full numerical calculation of the vortical energy fraction ϵ_{vort} as a function of the central overdensity δ_{max} , assuming an average shock Lorentz factor $\bar{\Gamma} = 100$ and a clump volume filling factor $N_{c,0}L^3 = 0.25$ (a different choice for this parameter would simply shift the curve). *Dotted line*: Analytical best-fit with the fitting function in eq. (33) and fitting parameters $c_1 \approx 0.176$ and $c_2 \approx 1.054$. The area between the *dashed lines* gives the region allowed by afterglow observations for the magnetic energy fraction ϵ_B .